8468 *Biochemistry* **2010,** *49,* 8468–8477
DOI: 10.1021/bi1008535

BIOCHEMISTRY
including biophysical chemistry & molecular biology
Article

NMR Characterization of Copper-Binding Domains 4−6 of ATP7B[†,‡]

Negah Fatemi,[§,⊥] Dmitry M. Korzhnev,[§,∥] Algirdas Velyvis,[§,∥] Bibudhendra Sarkar,*[,§,⊥] and Julie D. Forman-Kay*[,§,⊥]

[§]*Department of Biochemistry, and* [∥]*Departments of Chemistry and Medical Genetics, University of Toronto, Toronto, Ontario M5S 1A8, Canada, and* [⊥]*Program in Molecular Structure and Function, Hospital for Sick Children, Toronto, Ontario M5G 1X8, Canada*

Received May 26, 2010; Revised Manuscript Received August 19, 2010

ABSTRACT: The Wilson disease protein (ATP7B) is a copper-transporting member of the P-type ATPase superfamily, which plays a central role in copper homeostasis and interacts with the copper chaperone Atox1. The N-terminus of ATP7B is comprised of six copper-binding domains (WCBDs), each capable of binding one copper atom in the +1 oxidation state. To better understand the regulatory effect of copper binding to these domains, we have performed NMR characterization of WCBD4−6 (domains 4−6 of ATP7B). ^{15}N relaxation measurements on the apo and Cu(I)-bound WCBD4−6 show that there is no dramatic change in the dynamic properties of this three-domain construct; the linker between domains 4 and 5 remains flexible, domains 5 and 6 do not form a completely rigid dimer but rather have some flexibility with respect to each other, and there is minimal change in the relative orientation of the domains in the two states. We also show that, contrary to previous reports, the protein−protein interaction between Atox1 and the copper-binding domains takes place even in the absence of copper. Comparison of apo and Cu(I)-bound spectra of WCBD1−6 shows that binding of Cu(I) does not induce the formation of a unit that tumbles as a single entity, consistent with our results for WCBD4−6. We propose that copper transfer to and between the N-terminal domains of the Wilson Cu-ATPase occurs via protein interactions that are facilitated by the flexibility of the linkers and the motional freedom of the domains with respect to each other.

Copper is an essential trace element which plays an important role in mammalian cellular metabolism (*1*). While trace amounts of copper are needed to sustain life, excess copper is extremely toxic. Although various aspects of copper transport and metabolism have been investigated, many specific details of intracellular copper transport remain elusive. Cloning of the genes responsible for the two closely related major genetic disorders of copper metabolism in humans, Menkes disease (ATP7A) (*2*−*4*) and Wilson disease (ATP7B) (*5*−*7*), was a major breakthrough in the understanding of intracellular copper transport. Both genes encode copper-transporting P-type ATPases that play central roles in copper transport and homeostasis, using ATP to transport copper across the membrane against an electrochemical concentration gradient (*8*). Both transporters are localized to the trans-Golgi network where they receive copper from the copper delivery protein Atox1 (also known as HAH1) and transport it across the membrane for incorporation into copper-dependent enzymes (*9*−*11*). They also remove excess copper from the cytosol by vesicular trafficking to the plasma membrane in response to elevated intracellular copper levels (*12*−*14*).

ATP7A and ATP7B share certain core structural features with other members of the P-type ATPase family: a transmembrane domain, a nucleotide-binding domain, a phosphorylation domain, and an actuator domain (*8*). A crucial feature of the human copper-transporting ATPases is the presence of a large N-terminal segment, comprised of six copper-binding domains, each capable of binding one copper atom in the +1 oxidation state (*15*, *16*) in a cooperative manner (*15*, *17*). The six copper-binding domains have ferredoxin folds and are connected by linkers of various lengths. ATP7B performs its role by interacting with many cellular components in order to receive, transport, traffic, and excrete copper (*18*). ATP7B is known to interact with at least two proteins, the copper chaperone Atox1 (*19*−*21*) and COMMD1, which has been shown to bind copper in the Cu(II) state (*22*, *23*). In both cases, the N-terminal segment of ATP7B has been identified as the site of interaction. It has also been shown that this region interacts in a copper-dependent manner with the cytoplasmic nucleotide-binding/phosphorylation domain of ATP7B, with copper decreasing the interaction (*24*). An intact and functional N-terminal region is also required for the copper-induced phosphorylation of ATP7B (*25*) which is in turn required for vesicular trafficking (*26*). Mutations found within Wilson copper-binding domains (WCBD)[1] 1, 5, and 6 are known to give rise to Wilson disease (*27*) and show an impaired interaction with Atox1 (*19*), demonstrating their importance in ATP7B function. Domains 5

[†]This work was supported by funds from the Canadian Institutes of Health Research to J.D.F.-K. N.F. was supported by the Canadian Institutes of Health Research Strategic Training Program in the Structural Biology of Membrane Proteins Linked to Disease.

[‡]Resonance assignments for apo WCBD4−6 with BMRB ID 16937 have been deposited at the Biological Magnetic Resonance Bank.

*Corresponding authors. J.D.F.-K.: e-mail, forman@sickkids.ca; phone, (416) 813-5358; fax, (416) 813-5022. B.S.: e-mail, bsarkar@sickkids.ca; phone, (416) 813-5921; fax, (416) 813-5022.

[1]Abbreviations: NMR, nuclear magnetic resonance; WCBD, copper-binding domain of the Wilson copper transporter (ATP7B); MNK, metal-binding domain of the Menkes copper transporter (ATP7A); PCR, polymerase chain reaction; DTT, dithiothreitol; BCS, bathocuproinedisulfonic acid; EPR, electron paramagnetic resonance; ICP-AES, inductively coupled plasma−atomic emission spectrometry; DSS, 4,4-dimethyl-4-silapentane-1-sulfonic acid; TOCSY, total correlation spectroscopy; HSQC, heteronuclear single-quantum coherence; TROSY, transverse relaxation optimized spectroscopy; NOE, nuclear Overhauser effect; PDB, Protein Data Bank; SSP, secondary structure propensity.

 Published on Web 08/27/2010

and 6, the domains closest to the membrane spanning segment, have been shown to play a critical role for copper transport as well as copper-dependent intracellular trafficking of ATP7B (*28*). However, the mechanism by which these domains receive copper prior to transport across the membrane is not clear.

Investigations of the closely related Menkes protein ATP7A using a three-domain construct (MNK4−6) (*29*) and more recently on the entire N-terminal region (MNK1−6) (*30*) show that MNK1 and MNK4 form a stable adduct with Cu(I) Atox1 and are therefore likely the preferential sites for this interaction. On the other hand in ATP7B, domains 2 and 4 are thought to interact with Atox1 (*31*, *32*) showing that, although these two proteins are closely related, there are subtle yet significant differences in their N-terminal copper-binding domains. In a study involving the single-domain WCBD4 added to the two-domain WCBD5−6, it was shown that Atox1 can transfer copper through the formation of a stable adduct to WCBD4 but not WCBD5−6, and WCBD4 is able to transfer copper to WCBD5−6 (*31*). Further emphasizing the distinction between the Wilson and Menkes N-terminal region, these results are in contrast to the Menkes N-terminus, where domain 6 can bind metal independent of domain 4 (*30*). Until the recent characterization of entire N-terminal domain of ATP7B (*33*), which showed that all six domains can be metalated by Cu(I) Atox1, most studies focused on single or two-domain constructs (*31*, *34*). Dynamic information is available only for the two-domain constructs of WCBD5−6 in the apo state (*31*) and WCBD3−4 in the apo and Cu(I)-bound states (*34*). There has been no dynamic characterization of the entire WCBD1−6 nor of other constructs containing greater than two domains, with the exception of MNK4−6, which is lacking data from domain 5 in the Cu(I)-bound state (*29*).

In order to understand the mechanism of intracellular regulation and transport of copper, we chose to analyze an intact segment of the ATP7B N-terminal copper-binding domains spanning domains 4−6 (WCBD4−6). Interest in this particular construct stems from the inherent importance of domains 5 and 6 to copper transport and domain 4 as a target site for copper delivery from Atox1, with domains 4 and 5 joined by an uncharacterized flexible linker. We demonstrate the interaction of apo WCBD4−6 with apo Atox1 without the need for copper. We present the results of ^{15}N NMR relaxation studies of WCBD4−6 with coverage of three domains and the linker region in both the apo and Cu(I)-bound states. We show that the Cu(I)-binding domains of WCBD4−6 have independent mobility in the apo and the Cu(I)-bound state and that copper binding does not induce a change in the relative orientation of the domains with respect to one another. Comparison of NMR spectra of WCBD1−6 in the apo and Cu(I)-bound states suggests that domains 1−6 also retain some degree of flexibility with respect to one another, even in the Cu(I)-bound state. Thus, the flexibility of the N-terminal copper-binding domains with respect to each other appears to be an essential feature of the Wilson ATPase.

MATERIALS AND METHODS

Cloning, Purification, and NMR Sample Preparation of WCBD4−6. The DNA sequence encoding WCBD4−6 (amino acids 357−632 of ATP7B) was amplified via PCR and subcloned into a pET SUMO vector in *Escherichia coli* BL21 (DE3) cells. Cells were grown at 37 °C in M9 D_2O minimal media, supplemented with 10 mg/L biotin, 10 mg/L thiamin, 0.3% glucose (^{13}C-glucose was used in samples prepared for backbone assignment experiments), and 0.1% $^{15}NH_4Cl$. Expression of the fusion protein was induced at A_{600} of 0.6−0.8 by the addition of 0.1 mM IPTG for 18 h at 18 °C. Cells were harvested at 4420*g* for 15 min at 4 °C. The supernatant was poured off, and the bacterial pellets were either stored at −20 °C or lysed immediately. All buffers reported herein were prepared in such a way as to minimize cysteine oxidation: DTT-less solution was made, degassed under vacuum, purged with argon (for at least 30 min at room temperature), and then supplemented with DTT. Cell pellet was resuspended in binding buffer A (20 mM Tris-HCl, 500 mM NaCl, 10 mM imidazole, 2 mM DTT, pH 8, and 1 minitablet of EDTA-free Complete protease inhibitor cocktail per 100 mL of buffer A), lysed by sonication on ice for 5 × 1 min (pulsed), and centrifuged for 45 min at 118000*g* at 4 °C. The residual pellets were resuspended in the same buffer, sonicated, and centrifuged once more. The pooled supernatants were 0.8 μm filtered to remove cell debris and applied to a Ni^{2+} affinity column equilibrated with binding buffer A. After 1 h incubation at 4 °C while mixing, the column was washed extensively with the same buffer. The fusion protein was eluted with binding buffer A containing 500 mM imidazole. The eluate was allowed to digest with SUMO protease (Ulp) in the cold overnight. The digest was concentrated and applied to a Superdex-75 Hi-load gel-filtration column equilibrated with NMR sample buffer B (20 mM NaK-phosphate, 130 mM NaCl, 5 mM DTT, pH 6.0). Fractions corresponding to each protein were collected and concentrated in NMR sample buffer B.

Cloning, Purification, and NMR Sample Preparation of Atox1. The pGEX-6P-2 plasmid containing Atox1 was transformed into *E. coli* BL21 (DE3) cells, and the protein was expressed and purified according to previously described protocol (*35*) with a few changes. The fusion protein was digested on column according to standard protocol with PreScission protease. The flow-through containing Atox1 was concentrated, and as a final purification step, it was applied to a Superdex-75 Hi-load XK16/60 column (120 mL bed volume) equilibrated with NMR sample buffer B. Fractions corresponding to Atox1 were collected and concentrated in NMR sample buffer B.

Cloning, Purification, and NMR Sample Preparation of WCBD1−6. The DNA sequence encoding WCBD1−6 (amino acids 1−632 of ATP7B) was amplified via PCR and subcloned into a pGEX-6P-2 vector in *E. coli* BL21 (DE3) cells. One liter of cell culture was grown at 37 °C according to standard protocol. Protein expression was induced with 1 mM IPTG at room temperature for 16 h. The cells were harvested, and the cell pellet was resuspended in buffer C (100 mM NaH_2PO_4, 200 mM NaCl, 10 mM DTT, pH 7.0) and either stored at −20 °C or lysed immediately to extract protein.

Cells were thawed and incubated at room temperature with 1 mg/mL lysozyme for 15 min. One millimolar PMSF, 1 mM EDTA, and 1 minitablet of EDTA-free Complete protease inhibitor cocktail were added. Cells were lysed by sonication on ice, lysate was centrifuged for 30 min at 50000*g*, and filtered through a 0.8 μm filter to remove cell debris. Twenty milliliters of glutathione−Sepharose was equilibrated in buffer C and mixed with cleared lysate for 30 min at 4 °C. The suspension was drained, washed with 160 mL of buffer C supplemented with 10 g/L Triton X-100, and then washed with 140 mL of buffer C. Target protein was eluted in 40 mL of buffer C containing 10 mM reduced glutathione. Thirty units of PreScission protease was added to eluted protein, and the mixture was dialyzed against 2 L of buffer D (100 mM NaH_2PO_4, 200 mM NaCl, 5 mM DTT, pH 7.0) for 1 day in cold room. As the flow-through fraction from the glutathione−Sepharose resin

contained an appreciable amount of target protein, the glutathione affinity step was repeated on the flow-through fraction. Fifteen units of PreScission protease was added to protein obtained from repeat purification and likewise dialyzed against 2 L of buffer D for 1 day.

PreScission protease cleavage was continued for the second day in the freshly made 2 L of buffer D, after which dialysates were passed through to glutathione−Sepharose resin equilibrated in buffer C. The flow-through fraction containing the WCBD1−6 fragment was then dialyzed against 2 L of buffer E (50 mM NaH_2PO_4, 1 mM EDTA, 5 mM DTT, pH 7) overnight, loaded onto a 20 mL bed volume Q-Sepharose column, and eluted with a 400 mL gradient of 0−1 M NaCl in buffer E.

Fractions containing WCBD1−6 were pooled; 10% (w/w) glycerol and additional DTT to 20 mM were added. Into this solution solid urea was dissolved to 5.2 M solution, incubated for 30 min on ice, and dialyzed twice against 2 L of refolding buffer (buffer E with 10% v/v glycerol). Refolded WCBD1−6 was further purified on a Superdex 200 Hi-load XK16/60 column (120 mL bed volume) in 100 mM NaH_2PO_4, 200 mM NaCl, 1 mM DTT, and 20 mM BME. Relevant fractions were pooled and dialyzed against 1.1× concentration of NMR buffer F (50 mM NaH_2PO_4, 150 mM arginine, 1 mM EDTA, 10 mM DTT, pH 6.5).

Copper Loading of Protein Samples. Protein purification according to the above protocols typically yielded apo Atox1 containing no copper and "near-apo" WCBD4−6, which can contain as much as 8% copper, where 100% copper content would be equivalent to three copper atoms per protein molecule. Treatment with copper-specific chelator BCS (bathocuproine-disulfonic acid) followed by extensive dialysis did not affect the copper content of WCBD4−6. Protein concentrations were confirmed with amino acid analysis, and copper content of every Atox1 and WCBD4−6 sample was determined using the Cu(I) assay described by Brenner and Harris (*36*). EPR spectroscopy of the samples confirmed the absence of significant (<100 nM) concentrations of paramagnetic Cu(II) from the samples (Supporting Information) (*22*, *23*). WCBD1−6 as purified from *E. coli* cells, according to ICP-AES analysis, contains 0.35 copper atoms per protein molecule, or 0.35/6 = 0.058 copper per domain, if all copper atoms were distributed evenly across all six domains. It has been previously reported that all of the copper-binding domains have comparable affinities for binding copper (*37*) and that most are exchangeable except for one or two (*38*); for example, domain 2 retains copper in excess BCS (*39*). We therefore refer to Atox1, WCBD4−6, and WCBD1−6, as purified from *E. coli* cells minus the metal removal step described in previous protocols (*40*), as the apoprotein.

Copper loading of WCBD4−6 was achieved according to established protocols (*40*) using a 10-fold molar excess of $CuSO_4$ with DTT acting as a reductant. Precipitation was removed by centrifugation, and unbound copper was removed by dialysis in buffer A and gel filtration in NMR sample buffer B. WCBD4−6 NMR samples were 450−500 μM in 0.5 mL of NMR sample buffer B containing 0.5 mM DSS, 0.05% azide, 10 mM benzamidine, and 10% (v/v) D_2O and were sealed in an argon-blanketed NMR tube. Copper-loaded (1:1 molar ratio) Atox1 was prepared as was described for WCBD4−6.

WCBD1−6 was copper-loaded by adding 200 mM $CuCl_2$ in the presence of 20 mM DTT to achieve a 5-fold excess of copper over total binding sites. Precipitation was removed by centrifugation, and the sample was dialyzed overnight into 1.1× NMR sample buffer F.

NMR Spectroscopy. WCBD4−6 NMR spectra were acquired at 35 °C on four-channel Varian Unity Inova spectrometers operating at 500 and 600 MHz ^{1}H frequencies. Apo and Cu(I)-bound WCBD1−6 NMR spectra were acquired at 25 °C on four-channel Varian Unity Inova spectrometers operating at 500 MHz. HSQC spectra of apo WCBD4−6 and apo WCBD1−6 in NMR sample buffer B were also acquired at 45 °C at 500 MHz for comparative purposes. Data were processed using NMRPipe (*41*) and analyzed using NMRView (*42*).

Assignment Experiments. ^{1}HN, ^{15}N, ^{13}Cα, ^{13}Cβ, and ^{13}CO resonance assignments were performed on 500 μM apo WCBD4−6 using three-dimensional HNCO, HN(CA)CO, HNCA, HN(CO)CA, HNCACB, HN(CO)CACB, and (H)CC(CO)NH-TOCSY experiments (*43*).

NMR Cu Titrations of WCBD4−6. The Cu(I)-loaded state was assigned by titrating small amounts of copper and following the chemical shifts of cross-peaks. HSQC spectra were recorded at 500 MHz at 0, 200, 600, 1000, 1500, and 2000 μM $CuSO_4$. The NMR sample tube was sealed and argon-blanketed after each successive addition. To prevent dilution during the course of the titration, the NMR sample was concentrated as required to maintain a sample volume of approximately 0.5 mL and protein concentration of 500 μM.

NMR Titration of Apo WCBD4−6 with Atox1. Titrations were carried out at 35 °C using a 500 MHz spectrometer, and ^{15}N−^{1}H TROSY spectra were recorded at each point. The apo WCBD4−6 sample was at a concentration of 450 μM in a 450 μL volume. Apo Atox1 and Cu(I) Atox1 were added directly into the NMR tube containing the apo WCBD4−6 sample. Spectra were recorded after each addition at 0, 5, 10, 20, 50, 100, 275, 510, 700, 850, 1500, 1700, and 2600 μM for apo Atox1 and at 150, 225, 450, 900, 1350, and 3500 μM for Cu(I) Atox1. NMR samples were concentrated at several steps during the course of the titrations to maintain signal intensity and sample volumes of approximately 0.5 mL. To ensure that the interaction was fully saturated, titrations were performed to the point where no additional spectral changes were observed, indicating that titration end points for the apo Atox1 and Cu Atox1 titration had been reached. For the apo Atox1 titration, there were no changes beyond 1500 μM and no changes beyond 1350 μM for the Cu(I) Atox1 titration.

NMR Relaxation. ^{15}N T_1, $T_{1\rho}$, and heteronuclear ^{15}N{^{1}H} NOE measurements were performed as described elsewhere (*44*, *45*). Spectra of the apo and Cu(I)-loaded states were recorded at 35 °C at 600 MHz for T_1, $T_{1\rho}$, and heteronuclear NOE and at 500 MHz for T_1 and $T_{1\rho}$. Longitudinal T_1 and rotating frame $T_{1\rho}$ relaxation times and their uncertainties were obtained from exponential fits of peak intensities in a series of 2D ^{1}H−^{15}N correlation spectra using the DFIT module of the DASHA program (*46*). The resonances for about 30% of residues were excluded from the analysis due to spectral overlap. Transverse relaxation rates (R_2) were calculated from R_1 and $R_{1\rho}$ using the equation $R_{1\rho} = R_1 \cos^2\theta + R_2 \sin^2\theta$, where $\theta = \arctan(\omega_{SL}/\Delta\omega)$, $R_1 = 1/T_1$, and $R_{1\rho} = 1/T_{1\rho}$, $\Delta\omega$ is the resonance offset from the spin-lock carrier, and ω_{SL} is the spin-lock field strength (1779.4 and 1811.6 Hz at 500 MHz and 1953.1 and 1968.5 Hz at 600 MHz for the apo and Cu(I)-loaded samples, respectively). ^{15}N{^{1}H} steady-state NOE values were determined from the ratio of the intensities of the respective cross-peaks in ^{1}H−^{15}N correlation spectra obtained with and without proton saturation. Errors for the NOE values were determined from signal-to-noise ratios in spectra. To account for possible systematic errors in the experimental

data, minimal errors of 5% and 0.05 were assumed for R_1 and R_2 rates and NOE values, respectively.

The overall rotational correlation times (τ_c) and the rotational diffusion tensors of the individual domains of both the apo and Cu(I)-bound forms of WCBD4−6 were determined from ^{15}N R_1 and R_2 values using the program DASHA (*46*), which uses the model-free approach of Lipari and Szabo (*47*). For each domain, R_1 and R_2 data at 600 MHz from residues in rigid parts of the domains (those with NOE > 0.6) were globally fit to isotropic and asymmetric anisotropic models of overall rotation (*46*). The former model includes one parameter of molecular overall rotational diffusion, τ_c, while the later includes six parameters that describe anisotropic rotational diffusion, $\tau_c = 1/(2(D_x + D_y + D_z))$, D_x/D_z, D_y/D_z, where D_x, D_y, and D_z are eigenvalues of the rotational diffusion tensor and Euler angles α, β, and γ that orient the tensor within the PDB frame. The selection of the appropriate form of overall rotation using an *F*-test has shown that the anisotropic model is always required to properly fit the data. The structures of apo domains 3−4 (PDB id: 2rop) and apo domains 5−6 (PDB id: 2ew9) were used for the fit of the rotational diffusion models for domain 4 and domains 5 and 6, respectively.

Model-free analysis was performed on apo WCBD4−6 only due to a small inconsistency between 500 and 600 MHz data collected on the Cu(I)-bound protein. The inconsistency may be due to paramagnetic relaxation contributions from oxidation of Cu(I) to Cu(II). Bertini et al. (*48*) have documented the paramagnetic contribution of Cu(II) to ^{15}N R_2. For a protein with a 10 ns rotation correlation time, the paramagnetic contribution from Cu(II) at 5 Å distance is 3000−20000/s to ^{1}H R_2 and ~30−200/s to ^{15}N R_2 (~100 times less), in a 1 mM protein sample containing as little as 100 nM Cu(II). Therefore, in a 0.5 mM WCBD4−6 sample, as low as 50 nM Cu(II) may result in a 0.1/s contribution to ^{15}N R_2 values. Although precautions were taken to keep the oxidation of copper to a minimum during sample preparation, it could not be totally avoided once the NMR sample was placed in the magnet and experiments were begun.

Following the characterization of molecular overall rotation, the parameters of molecular rotational diffusion tensors of individual domains of apo WCBD4−6 were fixed and used in model-free analysis. The residues belonging to the flexible linkers were excluded from the analysis. ^{15}N R_1, R_2, and ^{15}N{^{1}H} NOE data at two magnetic fields (up to five experimental data per residue; see above) were fit using the following models of spectral density function including different number of parameters of internal motions (shown in brackets): {S^2}, {S^2, R_{ex}}, {S^2, τ_e}, {S^2, τ_e, R_{ex}}, and {S_s^2, S_f^2, τ_s}, where S^2 and S_s^2, S_f^2 ($S^2 = S_s^2, S_f^2$) are generalized order parameters, τ_e, τ_s are correlation times for the internal motions, and R_{ex} is the exchange contribution to transverse relaxation (at 500 MHz spectrometer) due to conformational exchange on microsecond to millisecond time scales. The order parameters reflect angular amplitudes of the internal motions of the amide bond vectors, while the correlation times reflect the time scale of the internal motions. In the original Lipari−Szabo approach order parameters S^2 and correlation times τ_e are used to characterize fast picosecond time scale dynamics (*47*). The theory was extended to account for internal motions on two time scales: picosecond with the correlation time τ_f and order parameter S_f^2 and subnanosecond with correlation time τ_s and order parameter S_s^2 (*49*). The model selection was performed based on the values of the χ^2 target function obtained in fits of relaxation data; more complex models were selected if they led to significant improvements in the fits (*F*-test confidence level of 0.25). Despite this relatively loose criterion for acceptance of more complex models assuming dynamics on micro to millisecond or subnanosecond time scales, the data for most of the residues indicate restricted mobility on the picosecond time scale consistent with the simplest spectral density models (see below).

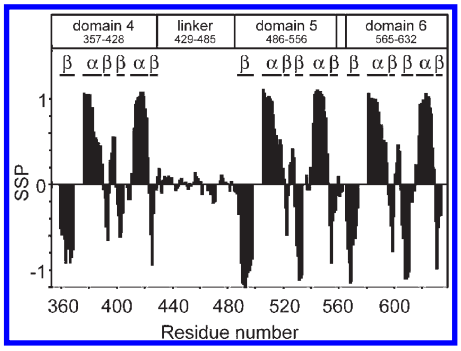

FIGURE 1: Secondary structure of apo WCBD4−6. Cα and Cβ and Co backbone chemical shifts were used in the SSP program (*50*) to generate a secondary structure propensity plot. In folded proteins, SSP values of +1 are expected for α-helical structure and −1 for β-strand structure. Domains 4, 5, and 6 are shown to have the $\beta\alpha\beta\beta\alpha\beta$ fold characteristic of heavy metal-associated domains.

RESULTS

Protein Structure Characterization. Triple resonance experiments were used to assign 88% of the non-proline ^{1}HN, ^{15}N, ^{13}CO, ^{13}Cα, and ^{13}Cβ chemical shifts for WCBD4−6, residues T357−A632 of ATP7B. Assignments for resonances (around the CXXC motif, in particular) were challenging due to degeneracy of the sequence in the three domains leading to overlap of signals. Secondary chemical shifts of the backbone ^{13}C nuclei are in agreement with those expected from previously published secondary structures of WCBD domains (*31*). Figure 1 shows the secondary structure propensity (SSP) values that combine different chemical shifts into a single residue-specific score of α-helical or β-strand population by calculating the weighted experimental chemical shift difference from random coil relative to that expected for stable helix or strand (*50*). As expected, each domain has the $\beta\alpha\beta\beta\alpha\beta$ fold seen in all heavy metal-associated domains including the previously published structures of WCBDs (*31*, *34*, *39*). The various secondary structure elements within each domain are numbered as follows: β1-L1-α1-L2-β2-L3-β3-L4-α2-L5-β4. Residues 357−428 comprise domain 4, 429−485 the flexible linker, 486−556 domain 5, and 565−632 domain 6. The residues connecting β-strands 2 and 3 also show some α-helical character but are part of a turn.

Effect of Cu(I) Binding on WCBD4−6. HSQC spectra were recorded at each point during the titration of apo WCBD4−6 with $CuSO_4$. This series of spectra made it possible to assign 79% of the non-proline backbone resonances of the Cu(I)-bound spectra and to detect chemical shifts in response to copper binding on a per residue basis. Again, assignments around the CXXC motif were more difficult. The ^{1}H and ^{15}N chemical shift differences between the apo and Cu(I)-bound protein are shown in Figure 2 as the weighted average chemical shift differences, $\Delta\delta = \{[(\Delta H)^2 + (\Delta N/5)^2]/2\}^{1/2}$, where ΔH and ΔN are chemical shift differences for ^{1}H and ^{15}N, respectively. Copper-loading of WCBD4−6 results in small chemical shift changes that are localized to the residues surrounding the copper binding sites, the CXXC motif, while the rest of the residues remain largely unaffected (Figure 2). These copper-dependent chemical shifts are observed for analogous

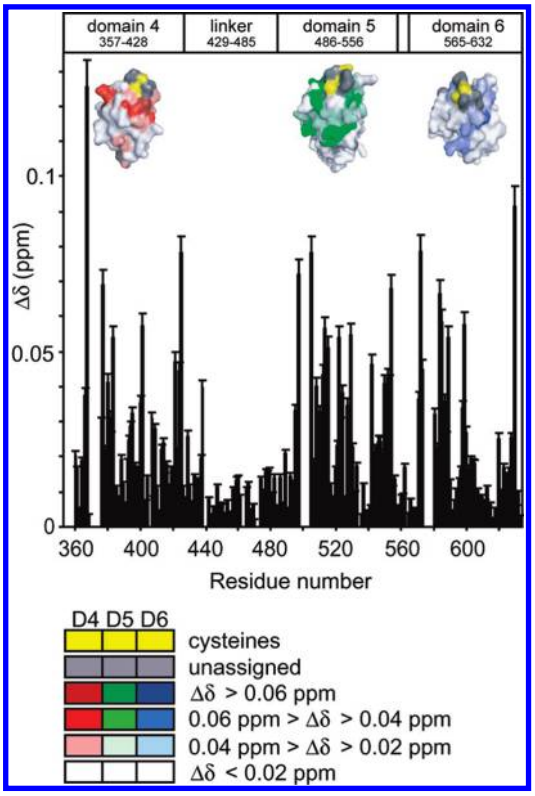

FIGURE 2: Cu(I) binding to WCBD4−6. Chemical shift differences between apo WCBD4−6 and Cu(I) WCBD4−6 are shown as a function of residue as well as mapped onto the surfaces of domain 4 (PDB id: 2rop) and domains 5 and 6 (PDB id: 2ew9). The surface having the greatest chemical shift differences for each of domains 4, 5, and 6 is displayed. Data for domains 5 and 6 are shown in different orientations of the surface of domains 5 and 6, with the orientation chosen for the domain 5 data completely obscuring domain 6. The domain graphics were created using the molecular graphics program PyMOL (*51*), using the scripts color_b.py and data2bfactor.py (provided by Dr. Robert L. Campbell). Surfaces of domains 4, 5, and 6 are shown in red-white, green-white, and blue-white gradients, respectively. The gradient is from dark to light with darkest shades showing a chemical shift of 0.06 ppm or greater and white for residues experiencing a chemical shift of 0.02 ppm or less. Unassigned residues are colored gray. Cysteine residues from the CXXC motif are shown in yellow: Cys 370 and Cys 373 in domain 4, Cys 499 and Cys 502 in domain 5, and Cys 575 and Cys 578 in domain 6.

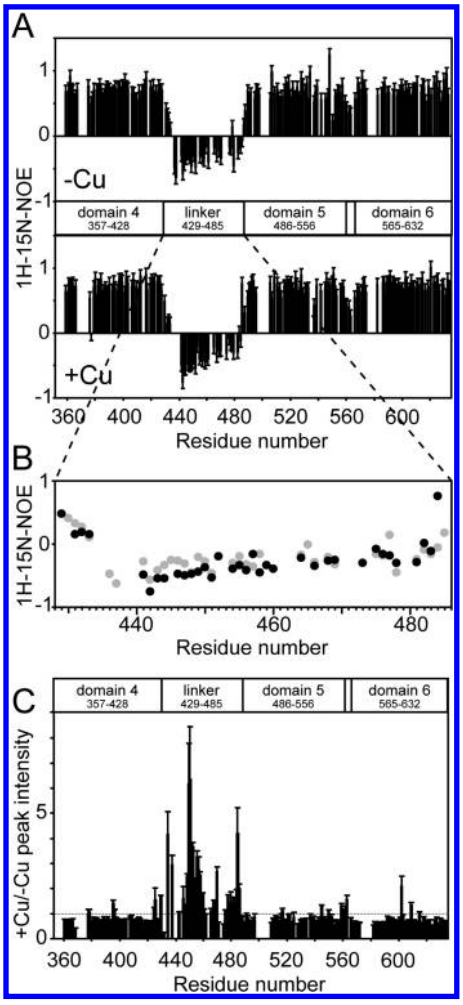

FIGURE 3: Effect of Cu(I) binding to WCBD4−6 on the flexible linker. $^{15}N\{^1H\}$ steady-state NOEs of apo WCBD4−6 and Cu(I) WCBD4−6 (A). An expansion of the linker regions shows lower NOE values in the Cu(I)-bound (black) than in the apo (gray) forms (B). The ratio of the peak intensities of the Cu(I)-bound to Cu(I)-free states of WCBD4−6 (C) shows that the flexible linker increases in flexibility in the Cu(I)-bound state. The dotted line (C) shows the peak intensity ratio = 1.

residues across the three domains. Shifts observed outside the immediate region of the CXXC motifs may be suggestive of transient interactions between the domains, consistent with the reported transfer of copper from domain 4 to a separate construct of domains 5 and 6 (*31*). While a quantitative comparison is not possible due to differences in temperature and buffer conditions, the chemical shifts observed for domain 4 in the context of WCBD4−6 change similarly upon copper binding to those observed for domain 4 in a domain 3 to 4 construct (*34*). Likewise, chemical shifts observed for domain 5 and domain 6 in WCBD4−6 change similarly upon copper binding to those seen for domains 5 and 6 in isolation (*31*). These observations suggest that when alone these domains bind copper in a similar fashion to when present together in the context in which they occur naturally.

The Flexible Linker Maintains Its Flexibility in both Apo and Cu(I)-Bound States. $^{15}N\{^1H\}$ steady-state NOEs of WCBD4−6 shown in Figure 3A indicate the presence of three stable domains and a long highly flexible linker E429−V485 which shows low NOE values, sharp resonances, and chemical shifts characteristic of disordered protein regions (e.g., $^1H^N$ chemical shifts around 8 ppm). This flexible linker joins domain 4 to domains 5 and 6 which are associated much more closely and are separated by a very short (but also somewhat flexible, according to NOE values) linker of only a few residues. The backbone chemical shifts measured for the linker region between domain 4 and domains 5 and 6 also indicate the lack of secondary structure in this region (Figure 1). Low NOE values suggest that the linker retains its flexibility in both the apo and Cu(I)-bound states (Figure 3A) and becomes even more mobile in the Cu(I)-bound state, based on the somewhat lower NOE values obtained for residues in the linker region in the Cu(I)-bound form of a protein (Figure 3B). As shown in Figure 3C, the resonances originating from the linker also show a significant increase in intensity due to a narrower line width when WCBD4−6 is Cu(I)-bound, in contrast to the ordered domains, which clearly demonstrates the enhanced flexibility in the linker region. Note that this effect is observable for WCBD4−6 samples which are loaded directly with copper or by copper titration.

Copper(I) Binding Does Not Change the Relative Orientation of Domains. The ^{15}N R_1 and R_2 relaxation rates and $^{15}N\{^1H\}$ NOE values are effective reporters of overall rotation

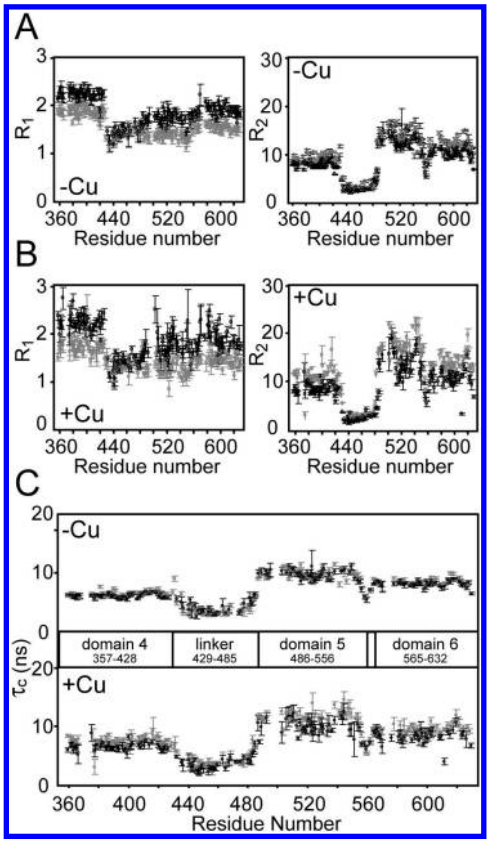

FIGURE 4: Dynamic properties of the WCBD4−6 residues in the apo and Cu(I)-bound states. R_1 and R_2 for WCBD4−6 residues in the apo (A) and Cu(I)-bound (B) states, in s^{-1}. Local effective correlation time (τ_c) calculated from ^{15}N R_2/R_1 ratios for individual amide groups in the apo and Cu(I)-bound state (C). Data were collected at 500 MHz (black) and 600 MHz (gray).

diffusion of the molecule and intermolecular motions of the internuclear N−H vectors, routinely used for characterization of the conformational flexibility of different protein regions. For relatively rigid residues, the measured relaxation data primarily reflect the overall tumbling of the molecule in solution. To further analyze the effects of Cu(I) binding to WCBD4−6, ^{15}N-spin relaxation data for apo WCBD4−6 and Cu(I) WCBD4−6 were measured. ^{15}N R_1 and R_2 rates and $^{15}N\{^1H\}$ NOE values for the apo and Cu(I)-loaded WCBD4−6, plotted in Figures 4A, 4B, and 3A, respectively, were used for characterization of fully asymmetric anisotropic rotational diffusion of individual domains of WCBD4−6 (Figure 5) and for the analysis of local intermolecular dynamics of the domains (Figure 6) (as described in Materials and Methods). Figure 4C shows correlation times (τ_c) obtained from ^{15}N R_2/R_1 ratios for individual residues of apo and Cu(I)-bound WCBD4−6. Figure 5 shows the τ_c and the parameters of the rotational diffusion tensor obtained from fitting R_1 and R_2 (at 600 MHz) using the fully anisotropic model. Domain 4 has the greatest motional freedom and a τ_c of ~6.3 ± 0.03 ns (N = 43) (Figure 5), where N is the number of residues used in calculations of the rotational diffusion tensor. The τ_c value of domain 4, while reflecting significant independent tumbling of this domain, is likely increased due to restriction of motion by the long flexible linker connecting it to domain 5; the effect of flexible linkers on the relaxation behavior of connected domains has recently been investigated by Wright et al. (*52*). Although the closely associated domains 5 and 6 have correlated motion due to the short linker joining them, they have flexibility with respect to one another

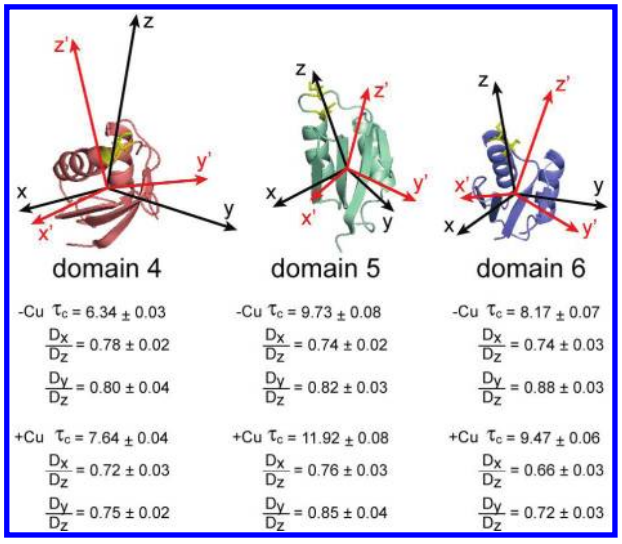

FIGURE 5: Rotational diffusion tensors of the apo and Cu(I)-bound domains 4, 5, and 6 in the apo and Cu(I)-bound states. Directions of principle axes of the diffusion tensors in the apo (black) and Cu(I)-bound (red) states mapped onto the structures of domains 4, 5, and 6. Rotational correlation times and parameters of rotational anisotropy in both states are provided below each domain.

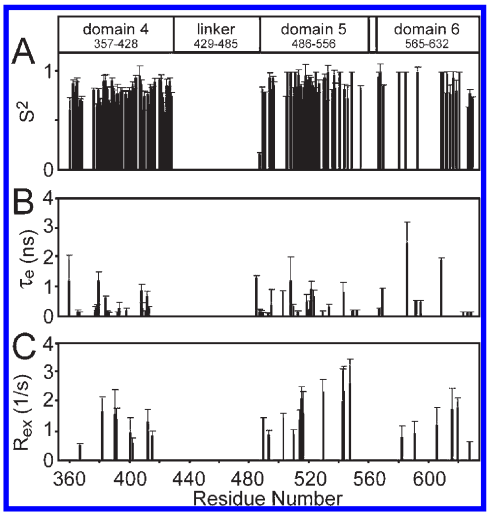

FIGURE 6: Model-free parameters for the local motion of the backbone amide N−H of domains 4, 5, and 6 in the apo state. S^2, the squared generalized order parameter (A), τ_e, internal motion correlation time (in nanoseconds) (B), and R_{ex}, exchange rate (in reciprocal seconds) (C) are plotted as a function of the residue number. Values are not shown for residues whose relaxation could not be measured accurately (due to signal overlap) or for the flexible linker region. The S^2 (A) and τ (B) data shown for residues fit using the $\{S_s^2, S_f^2, \tau_s\}$ model are $S^2 = S_s^2 S_f^2$ and τ_s, respectively.

based on differences in their correlation times, 9.7 ± 0.08 ns (N = 32) for domain 5 and 8.2 ± 0.07 ns (N = 32) for domain 6 (see Figure 5). This is in contrast to a previous report that the isolated domain 5 and 6 construct tumbles as a rigid dumbbell (*31*) but in agreement with molecular dynamic simulations suggesting the N-terminal metal-binding domains of related ATPases have motional freedom to reorient with respect to one another depending on the length of their linkers (*53*). Each of the three domains and the linker region display distinct rotation correlation times in the apo state (Figure 4C), suggesting that the domains reorient at different rates, are flexible with respect to each other, and do not tumble as a single large protein. The R_1, R_2, and τ_c for the domains do not show large changes between the apo and Cu(I)-loaded WCBD4−6

(Figure 4C), indicating that the overall dynamics of WCBD4−6 in the apo and Cu(I)-bound states remain the same in the two states.

Rotational diffusion tensors of the apo and Cu(I)-bound domains 4, 5, and 6 are shown in Figure 5. Tensors are nearly axially symmetric ($D_x/D_z \approx D_y/D_z$), and the parameters of rotational anisotropy (D_x/D_z and D_y/D_z) are similar in both the apo and the Cu(I)-bound states. The directions of principal axes of the rotational diffusion tensors are similar in both the apo and the Cu(I)-bound states; the directions of Z axes between apo and Cu(I)-bound forms differ by no more than 23 degrees for domain 4, 29 degrees for domain 5, and 28 degrees for domain 6. Together with the similar (although not identical) overall rotational correlation times for individual domains in apo and Cu(I)-bound states, the data show that the relative orientations and mobilities of the domains in WCBD4−6 do not change significantly upon binding copper.

^{15}N relaxation data were analyzed by model-free analysis assuming a fully asymmetric rotational diffusion tensor. The model-free parameters S^2, τ_e, and R_{ex} for apo WCBD4−6 are shown in Figure 6. Most residues from folded domains have order parameters $S^2 > 0.6$, indicating that the internal motions in the domains are restrained on the picosecond to nanosecond time scales. Slightly lower order parameters of $S^2 \approx 0.5$ were observed for four residues in domain 4: I408 and E423 in loops L4 and L5, respectively, and I390 and E412 in β2 and α2, respectively. Motions on pico- to nanosecond time scales with correlation times (τ_e or τ_s) in the range 0.07−2.4 ns were detected for 17 residues in domain 4, 20 residues in domain 5, and 9 residues in domain 6. Conformational exchange terms (R_{ex}) of up to 2.6/s pointing to micro- to millisecond time scale dynamics, were detected for 8 residues in domain 4, 11 residues in domain 5, and 6 residues in domain 6. The first residue of the defined boundaries for domain 5, A486, has a low order parameter (S^2 of 0.2) and higher internal correlation time (τ_s = 1.3 ns), which demonstrates that it is part of the long flexible linker connecting domains 4 and 5. Note that model-free parameters for the Cu(I)-bound state are not reported due to inconsistencies in the data (see Materials and Methods).

Protein−Protein Interactions with Atox1. HSQC spectra can be used to map protein−protein interaction surfaces at residue-level resolution, by monitoring the perturbation in the positions or intensities of the resonances upon titration of a binding partner. Apo Atox1 and Cu(I) Atox1 were titrated into apo WCBD4−6 with final spectra representing fully saturated complexes (see Materials and Methods). The final titration points contain an excess of Atox1 to WCBD4−6, 5.8:1 and 7.8:1 for apo Atox1 and Cu(I) Atox1, respectively. The titration with apo Atox1 into apo WCBD4−6 shows that an interaction is detectable in the absence of Cu(I) or in the presence of the very low levels of Cu(I) (see Materials and Methods). Chemical shift differences between apo WCBD4−6 and each saturated complex (final titration point) shown in Figure 7 are weighted average chemical shift differences calculated in a similar manner as those shown in Figure 2 for Cu(I) binding. Significant chemical shift changes are observed for domain 4 and to a lesser extent for domain 5 (Figure 7A). The linker region and domain 6 show no chemical shift changes. This interaction pattern is consistent with previously published results showing a complex in fast exchange between Atox1 and WCBD4 in the presence of Cu(I) (*31*). This is also in agreement with recent work on titration of domains 1−6 with Cu(I) Atox1 (*33*) showing a differential interaction of

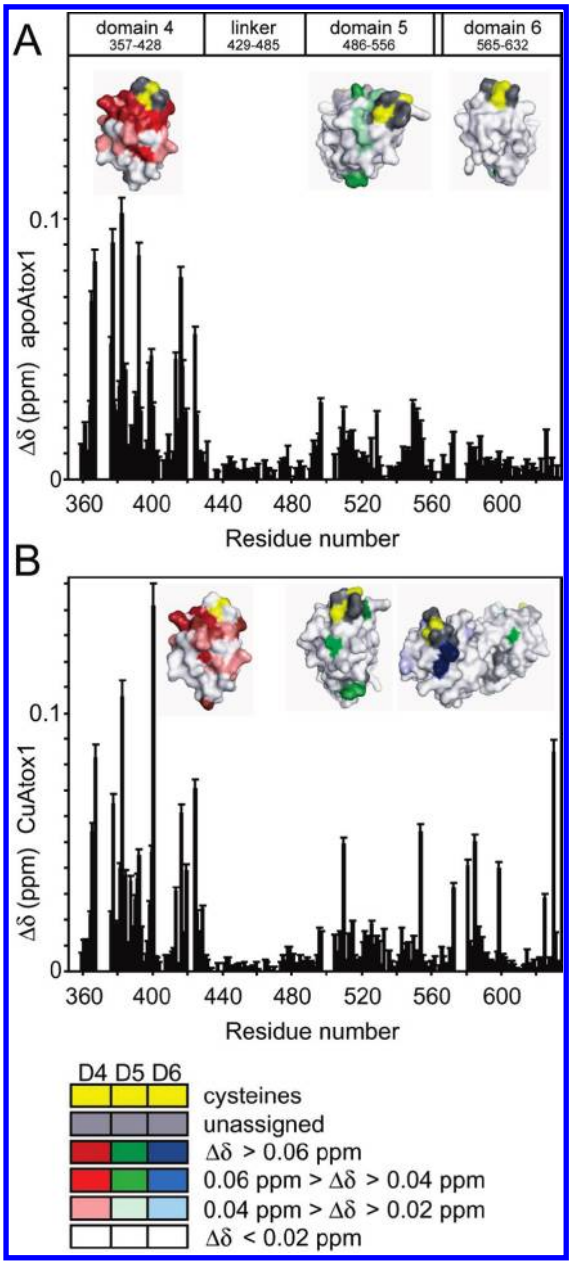

FIGURE 7: Interaction of apo WCBD4−6 with apo and Cu(I) Atox1. Chemical shift differences between apo WCBD4−6 and apo WCBD4−6 in a fully saturated complex with apo Atox1 (molar ratio 1:5.8) (A). Chemical shift differences between apo WCBD4−6 and apo WCBD4−6 in a fully saturated complex with Cu(I) Atox1 (molar ratio 1:7.8) (B). Differences between initial and end points of the titration are shown as a function of residue as well as mapped onto the surfaces of the structures of domain 4 and domains 5 and 6 as for Figure 2, with the orientation chosen for the domain 5 data obscuring domain 6 in both (A) and (B) and the orientation for domain 6 data obscuring domain 5 in (A).

domain 4 versus domains 5 and 6, although that study did not show binding in the absence of copper. Our chemical shift changes for WCBD4−6 interaction with apo Atox1 (Figure 7A) are only somewhat smaller than those measured for Cu(I) Atox1 (Figure 7B), suggesting that the interaction between Atox1 and WCBD4−6 is driven primarily by protein−protein interactions and that the presence of Cu(I), while not required, does lead to enhanced binding.

When WCBD4−6 binds Cu(I) Atox1 (Figure 7B), presumably enabling Cu(I) transport, the residues affected are very different from residues involved in the binding of free copper (Figure 2).

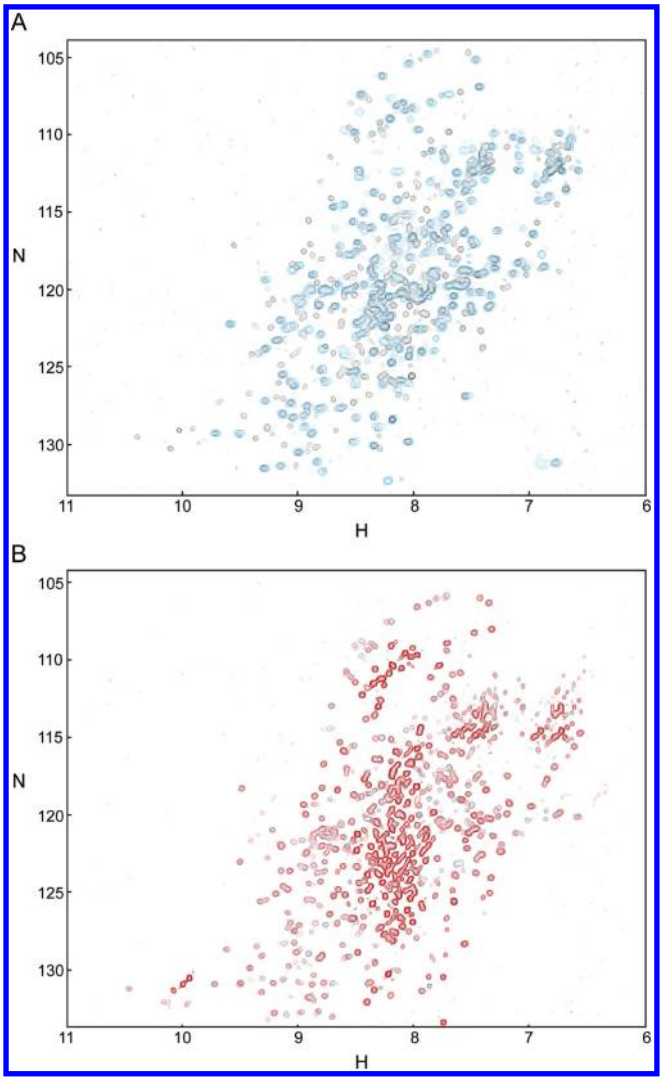

FIGURE 8: WCBD1−6 spectra in apo and Cu(I)-bound states. HSQC spectra (45 °C) of apo WCBD4−6 (blue) and apo WCBD4−6 (black) show overlap in a significant number of peaks (A). TROSY spectra (25 °C) of WCBD1−6 in the apo (black) and Cu(I)-bound states (red) is typical of smaller molecules with high mobility (A).

These data suggest that the targeting of copper by Atox1 to domain 4 is driven by favorable protein−protein interactions; this is further supported by the interaction of Atox1 even in the apo state with domain 4 (Figure 7A). Our findings are consistent with the data for MNK4−6 and MNK1−6 showing that domain 4 is the domain that receives copper from Atox1 (*29*, *30*).

Copper(I) Binding to WCBD1−6 Does Not Appear To Induce a Significant Change in Relative Mobility of Domains. Comparison of spectra of apo WCBD1−6 to those of apo WCBD4−6 demonstrates overlap of many of the resonances (Figure 8A), indicative of limited interactions between domains 1−3 and 4−6. The spectra for domains 1−6 in the apo and Cu(I)-bound states are overlaid in Figure 8B, with the large degree of overlap suggestive of similar overall behavior in the absence and presence of copper. Visual inspection of WCBD1−6 spectra in both states reveals sharp peaks having line shapes typical of smaller proteins with reasonably rapid overall tumbling. The assignment of NMR resonances of N-terminal copper-binding domains 1−6 of ATP7B, a 72 kDa protein, by Banci et al (*33*) without the need for specialized methods for "large" protein NMR (*54*, *55*) also argues for significant motional flexibility. These observations are inconsistent with WCBD1−6 tumbling as a single unit in either apo or copper-bound states. Correlated motions of domains 5 and 6, consistent with the results for WCBD4−6, are expected, and it is possible that motions of additional domains are also correlated. Overall, however, the results are supportive of a model in which the binding of copper to WCBD1−6 leaves the domains largely flexible with respect to one another.

DISCUSSION

Many proteins contain multiple binding domains connected by linkers. These multiple domains can participate in interdomain motions that play a key role in molecular recognition and regulation. The WCBD N-terminal region of ATP7B contains six copper-binding domains joined through linkers of various lengths and flexibility. These domains are involved in many aspects of copper metabolism. WCBD receives copper through interaction with the copper chaperone Atox1 (*19*−*21*) and binds copper in a cooperative manner (*15*, *40*). There have been many studies alluding to a conformational change or transition in the N-terminal region domains of both the Wilson (*15*, *40*) and the Menkes ATPase (*15*, *16*, *56*, *57*) upon copper binding. In order to more specifically characterize the conformational transitions that have been suggested to take place upon binding copper and to detect interactions with protein partners that can ultimately regulate copper transport by ATP7B, we have employed NMR spectroscopy to probe the structural and dynamic properties of WCBD4−6, metal-binding domains 4−6 of the N-terminal metal-binding domain of ATP7B, as well as to describe WCBD1−6, the full N-terminal domain.

Our results reveal that the three domains in WCBD4−6 have independent mobility in solution. Domain 4 tumbles independently and is connected by a long flexible linker to domains 5 and 6 which are joined only by a very short linker and tumble with some flexibility with respect to each other (Figure 3A,B). Analysis of the correlation times for WCBD4−6 (Figures 4 and 5) suggests that domains 4, 5, and 6 tumble as separate entities in the apo state and Cu(I)-bound state, with distinct τ_c values of 6.3 ± 0.03, 9.7 ± 0.08, and 8.2 ± 0.07 ns, respectively (Figure 5). The closely associated domains 5 and 6 have different correlation times (9.7 ± 0.08 and 8.2 ± 0.07 ns, respectively; see Figure 5) and, therefore, have flexibility with respect to one another which is in contrast to that reported previously for the isolated domain 5 to 6 construct (*31*). The correlation times for domains 4 and 5 are larger than those previously reported for isolated domain 6 and domains 5 and 6 (4.5 and 9.1 ns, respectively, at 25 °C (*31*)), with the long flexible linker connecting domain 4 to domain 5 possibly leading to an increase in the correlation times (*52*). This linker effect may also contribute to the reported increases in R_2 values for residues of domain 5 of the ATP7A domains 4−6 (*29*).

Our relaxation analysis of WCBD4−6 shows no evidence in support of significant copper-dependent conformational change due to the rearrangement or reorientation of domains 4, 5, and 6 relative to each other (Figure 5). The fairly sharp resonances of WCBD1−6 in the apo and Cu(I)-bound states (Figure 8B) point to domains that do not tumble as a single unit but instead are somewhat flexible with respect to each other, as in WCBD4−6. Importantly, copper binding to WCBD1−6 does not induce the formation of a larger uniformly tumbling globular unit as there is no drastic change in the overall dynamic character of the N-terminal domains upon binding Cu(I). Secondary and tertiary

conformational changes reported by Didonato et al. (*15*, *40*) in WCBD1−6 by the binding of copper are probably due to the effect of copper binding on residues within each domain as detected by the chemical shift changes in our Cu(I)-binding experiments on domains 4−6. In addition we find that, even in the absence of copper, Atox1 interacts preferentially with domain 4, which has greater motional freedom than domains 5 and 6.

Based on these data and the work of others on the metal-binding domains of ATP7B and ATP7A (*30*, *33*, *53*, *58*), the flexibility between the domains in the apo and Cu(I)-bound state appears to be a key feature of the N-terminal region of multidomain Cu-ATPases and copper binding. Domain−domain flexibility in this region provides motional freedom to the domains that, by increasing their accessibility, could facilitate protein−protein interactions with the copper chaperone Atox1 in order to receive copper and to subsequently transfer copper to the other N-terminal copper-binding domains and finally to the transmembrane site for transport across the membrane. The idea of a transition from disorder and flexibility to order upon binding has long been a central paradigm in protein structure and dynamics; in fact, the stabilization of tertiary structure by metal binding is a key feature of metalloregulatory proteins (*59*). Nevertheless, there are examples of retention of dynamics or even increases in motion upon binding (*60*, *61*). This appears to be another such example, with retained flexibility and relative conformation freedom between the domains, creating an ensemble of states that may facilitate the multistep process of copper transport by copper-transporting ATPases.

ACKNOWLEDGMENT

We thank L. E. Kay and R. Muhandiram for assistance with NMR experiments.

SUPPORTING INFORMATION AVAILABLE

EPR spectra. This material is available free of charge via the Internet at http://pubs.acs.org.

REFERENCES

1. Sarkar, B. (1999) Treatment of Wilson and Menkes Diseases. *Chem. Rev. 99*, 2535–2544.
2. Chelly, J., Tumer, Z., Tonnesen, T., Petterson, A., Ishikawa-Brush, Y., Tommerup, N., Horn, N., and Monaco, A. P. (1993) Isolation of a candidate gene for Menkes disease that encodes a potential heavy metal binding protein. *Nat. Genet. 3*, 14–19.
3. Mercer, J. F., Livingston, J., Hall, B., Paynter, J. A., Begy, C., Chandrasekharappa, S., Lockhart, P., Grimes, A., Bhave, M., and Siemieniak, D.; et al. (1993) Isolation of a partial candidate gene for Menkes disease by positional cloning. *Nat. Genet. 3*, 20–25.
4. Vulpe, C., Levinson, B., Whitney, S., Packman, S., and Gitschier, J. (1993) Isolation of a candidate gene for Menkes disease and evidence that it encodes a copper-transporting ATPase. *Nat. Genet. 3*, 7–13.
5. Bull, P. C., Thomas, G. R., Rommens, J. M., Forbes, J. R., and Cox, D. W. (1993) The Wilson disease gene is a putative copper transporting P-type ATPase similar to the Menkes gene. *Nat. Genet. 5*, 327–337.
6. Tanzi, R. E., Petrukhin, K., Chernov, I., Pellequer, J. L., Wasco, W., Ross, B., Romano, D. M., Parano, E., Pavone, L., and Brzustowicz, L. M.; et al. (1993) The Wilson disease gene is a copper transporting ATPase with homology to the Menkes disease gene. *Nat. Genet. 5*, 344–350.
7. Petrukhin, K., Fischer, S. G., Pirastu, M., Tanzi, R. E., Chernov, I., Devoto, M., Brzustowicz, L. M., Cayanis, E., Vitale, E., and Russo, J. J.; et al. (1993) Mapping, cloning and genetic characterization of the region containing the Wilson disease gene. *Nat. Genet. 5*, 338–343.
8. Axelsen, K. B., and Palmgren, M. G. (1998) Evolution of substrate specificities in the P-type ATPase superfamily. *J. Mol. Evol. 46*, 84–101.
9. Dierick, H. A., Adam, A. N., Escara-Wilke, J. F., and Glover, T. W. (1997) Immunocytochemical localization of the Menkes copper transport protein (ATP7A) to the trans-Golgi network. *Hum. Mol. Genet. 6*, 409–416.
10. Schaefer, M., Roelofsen, H., Wolters, H., Hofmann, W. J., Muller, M., Kuipers, F., Stremmel, W., and Vonk, R. J. (1999) Localization of the Wilson's disease protein in human liver. *Gastroenterology 117*, 1380–1385.
11. La Fontaine, S., and Mercer, J. F. (2007) Trafficking of the copper-ATPases, ATP7A and ATP7B: Role in copper homeostasis. *Arch. Biochem. Biophys. 463*, 149–167.
12. Schaefer, M., Hopkins, R. G., Failla, M. L., and Gitlin, J. D. (1999) Hepatocyte-specific localization and copper-dependent trafficking of the Wilson's disease protein in the liver. *Am. J. Physiol. 276*, G639–646.
13. Roelofsen, H., Wolters, H., Van Luyn, M. J., Miura, N., Kuipers, F., and Vonk, R. J. (2000) Copper-induced apical trafficking of ATP7B in polarized hepatoma cells provides a mechanism for biliary copper excretion. *Gastroenterology 119*, 782–793.
14. Petris, M. J., Mercer, J. F., Culvenor, J. G., Lockhart, P., Gleeson, P. A., and Camakaris, J. (1996) Ligand-regulated transport of the Menkes copper P-type ATPase efflux pump from the Golgi apparatus to the plasma membrane: a novel mechanism of regulated trafficking. *EMBO J. 15*, 6084–6095.
15. DiDonato, M., Narindrasorasak, S., Forbes, J. R., Cox, D. W., and Sarkar, B. (1997) Expression, purification, and metal binding properties of the N-terminal domain from the wilson disease putative copper-transporting ATPase (ATP7B). *J. Biol. Chem. 272*, 33279–33282.
16. Ralle, M., Cooper, M. J., Lutsenko, S., and Blackburn, N. J. (1998) The Menkes disease protein binds copper via novel 2-coordinate Cu(I)-cysteinates in the N-terminal domain. *J. Am. Chem. Soc. 120*, 13525–13526.
17. Jensen, P. Y., Bonander, N., Moller, L. B., and Farver, O. (1999) Cooperative binding of copper(I) to the metal binding domains in Menkes disease protein. *Biochim. Biophys. Acta 1434*, 103–113.
18. Fatemi, N., and Sarkar, B. (2002) Structural and functional insights of Wilson disease copper-transporting ATPase. *J. Bioenerg. Biomembr. 34*, 339–349.
19. Hamza, I., Schaefer, M., Klomp, L. W., and Gitlin, J. D. (1999) Interaction of the copper chaperone HAH1 with the Wilson disease protein is essential for copper homeostasis. *Proc. Natl. Acad. Sci. U.S.A. 96*, 13363–13368.
20. Larin, D., Mekios, C., Das, K., Ross, B., Yang, A. S., and Gilliam, T. C. (1999) Characterization of the interaction between the Wilson and Menkes disease proteins and the cytoplasmic copper chaperone, HAH1p. *J. Biol. Chem. 274*, 28497–28504.
21. Hamza, I., Prohaska, J., and Gitlin, J. D. (2003) Essential role for Atox1 in the copper-mediated intracellular trafficking of the Menkes ATPase. *Proc. Natl. Acad. Sci. U.S.A. 100*, 1215–1220.
22. Peisach, J., and Blumberg, W. E. (1974) Structural implications derived from the analysis of electron paramagnetic resonance spectra of natural and artificial copper proteins. *Arch. Biochem. Biophys. 165*, 691–708.
23. Narindrasorasak, S., Kulkarni, P., Deschamps, P., She, Y. M., and Sarkar, B. (2007) Characterization and copper binding properties of human COMMD1 (MURR1). *Biochemistry 46*, 3116–3128.
24. Tsivkovskii, R., MacArthur, B. C., and Lutsenko, S. (2001) The Lys1010-Lys1325 fragment of the Wilson's disease protein binds nucleotides and interacts with the N-terminal domain of this protein in a copper-dependent manner. *J. Biol. Chem. 276*, 2234–2242.
25. Vanderwerf, S. M., Cooper, M. J., Stetsenko, I. V., and Lutsenko, S. (2001) Copper specifically regulates intracellular phosphorylation of the Wilson's disease protein, a human copper-transporting ATPase. *J. Biol. Chem. 276*, 36289–36294.
26. Cater, M. A., La Fontaine, S., and Mercer, J. F. (2007) Copper binding to the N-terminal metal-binding sites or the CPC motif is not essential for copper-induced trafficking of the human Wilson protein (ATP7B). *Biochem. J. 401*, 143–153.
27. Loudianos, G., Dessi, V., Lovicu, M., Angius, A., Nurchi, A., Sturniolo, G. C., Marcellini, M., Zancan, L., Bragetti, P., Akar, N., Yagci, R., Vegnente, A., Cao, A., and Pirastu, M. (1998) Further delineation of the molecular pathology of Wilson disease in the Mediterranean population. *Hum. Mutat. 12*, 89–94.
28. Cater, M. A., Forbes, J., La Fontaine, S., Cox, D., and Mercer, J. F. (2004) Intracellular trafficking of the human Wilson protein: the role of the six N-terminal metal-binding sites. *Biochem. J. 380*, 805–813.
29. Banci, L., Bertini, I., Cantini, F., Chasapis, C. T., Hadjiliadis, N., and Rosato, A. (2005) A NMR study of the interaction of a three-domain construct of ATP7A with copper(I) and copper(I)-HAH1: the interplay of domains. *J. Biol. Chem. 280*, 38259–38263.

30. Banci, L., Bertini, I., Cantini, F., Della-Malva, N., Migliardi, M., and Rosato, A. (2007) The different intermolecular interactions of the soluble copper-binding domains of the menkes protein, ATP7A. *J. Biol. Chem. 282*, 23140–23146.
31. Achila, D., Banci, L., Bertini, I., Bunce, J., Ciofi-Baffoni, S., and Huffman, D. L. (2006) Structure of human Wilson protein domains 5 and 6 and their interplay with domain 4 and the copper chaperone HAH1 in copper uptake. *Proc. Natl. Acad. Sci. U.S.A. 103*, 5729–5734.
32. van Dongen, E. M., Klomp, L. W., and Merkx, M. (2004) Copper-dependent protein-protein interactions studied by yeast two-hybrid analysis. *Biochem. Biophys. Res. Commun. 323*, 789–795.
33. Banci, L., Bertini, I., Cantini, F., Massagni, C., Migliardi, M., and Rosato, A. (2009) An NMR study of the interaction of the N-terminal cytoplasmic tail of the Wilson disease protein with copper(I)-HAH1. *J. Biol. Chem. 284*, 9354–9360.
34. Banci, L., Bertini, I., Cantini, F., Rosenzweig, A. C., and Yatsunyk, L. A. (2008) Metal binding domains 3 and 4 of the Wilson disease protein: solution structure and interaction with the copper(I) chaperone HAH1. *Biochemistry 47*, 7423–7429.
35. Narindrasorasak, S., Zhang, X., Roberts, E. A., and Sarkar, B. (2004) Comparative analysis of metal binding characteristics of copper chaperone proteins, Atx1 and ATOX1. *Bioinorg. Chem. Appl. 2*, 105–123.
36. Brenner, A. J., and Harris, E. D. (1995) A quantitative test for copper using bicinchoninic acid. *Anal. Biochem. 230*, 360.
37. Wernimont, A. K., Yatsunyk, L. A., and Rosenzweig, A. C. (2004) Binding of copper(I) by the Wilson disease protein and its copper chaperone. *J. Biol. Chem. 279*, 12269–12276.
38. Walker, J. M., Tsivkovskii, R., and Lutsenko, S. (2002) Metallochaperone Atox1 transfers copper to the NH2-terminal domain of the Wilson's disease protein and regulates its catalytic activity. *J. Biol. Chem. 277*, 27953–27959.
39. Walker, J. M., Huster, D., Ralle, M., Morgan, C. T., Blackburn, N. J., and Lutsenko, S. (2004) The N-terminal metal-binding site 2 of the Wilson's disease protein plays a key role in the transfer of copper from Atox1. *J. Biol. Chem. 279*, 15376–15384.
40. DiDonato, M., Hsu, H. F., Narindrasorasak, S., Que, L., Jr., and Sarkar, B. (2000) Copper-induced conformational changes in the N-terminal domain of the Wilson disease copper-transporting ATPase. *Biochemistry 39*, 1890–1896.
41. Delaglio, F., Grzesiek, S., Vuister, G. W., Zhu, G., Pfeifer, J., and Bax, A. (1995) NMRPipe: a multidimensional spectral processing system based on UNIX pipes. *J. Biomol. NMR 6*, 277–293.
42. Johnson, B. A., and Blevins, R. A. (1994) NMRView: a computer program for the visualization and analysis of NMR data. *J. Biomol. NMR 4*, 603–614.
43. Cavanagh, J., Fairbrother, W. J., Palmer, A. G., III, Rance, M., and Skelton, N. J. (2007) in Protein NMR spectroscopy: Principles and practice, 2nd ed., pp 613−655, Academic Press, San Diego, CA.
44. Farrow, N. A., Muhandiram, R., Singer, A. U., Pascal, S. M., Kay, C. M., Gish, G., Shoelson, S. E., Pawson, T., Forman-Kay, J. D., and Kay, L. E. (1994) Backbone dynamics of a free and phosphopeptide-complexed Src homology 2 domain studied by ^{15}N NMR relaxation. *Biochemistry 33*, 5984–6003.
45. Korzhnev, D. M., Skrynnikov, N. R., Millet, O., Torchia, D. A., and Kay, L. E. (2002) An NMR experiment for the accurate measurement of heteronuclear spin-lock relaxation rates. *J. Am. Chem. Soc. 124*, 10743–10753.
46. Orekhov, V. Y., Nolde, D. E., Golovanov, A. P., Korzhnev, D. M., and Arseniev, A. S. (1995) Processing of heteronuclear NMR relaxation data with the new software DASHA. *Appl. Magn. Reson. 9*, 581–588.
47. Lipari, G., and Szabo, A. (1982) Model-free approach to the interpretation of nuclear magnetic resonance relaxation in macromolecules. *J. Am. Chem. Soc. 104*, 4546–4559.
48. Bertini, I., Luchinat, C., and Parigi, G. (2001) Solution NMR of paramagnetic molecules, in Current Methods in Inorganic Chemistry, p 84 (Table 83.81), Elsevier Science, Amsterdam.
49. Clore, G. M., Szabo, A., Bax, A., Kay, L. E., Driscoll, P. C., and Gronenborn, A. M. (1990) Deviations from the simple two-parameter model-free approach to the interpretation of nitrogen-15 nuclear magnetic relaxation of proteins. *J. Am. Chem. Soc. 112*, 4989–4991.
50. Marsh, J. A., Singh, V. K., Jia, Z., and Forman-Kay, J. D. (2006) Sensitivity of secondary structure propensities to sequence differences between alpha- and gamma-synuclein: implications for fibrillation. *Protein Sci. 15*, 2795–2804.
51. DeLano, W. L. (2008) DeLano Scientific LLC, Palo Alto, CA.
52. Bae, S. H., Dyson, H. J., and Wright, P. E. (2009) Prediction of the rotational tumbling time for proteins with disordered segments. *J. Am. Chem. Soc. 131*, 6814–6821.
53. Sharma, S., and Rosato, A. (2009) Role of the N-terminal tail of metal-transporting P(1B)-type ATPases from genome-wide analysis and molecular dynamics simulations. *J. Chem. Inf. Model. 49*, 76–83.
54. Tugarinov, V., Hwang, P. M., and Kay, L. E. (2004) Nuclear magnetic resonance spectroscopy of high-molecular-weight proteins. *Annu. Rev. Biochem. 73*, 107–146.
55. Tugarinov, V., Kanelis, V., and Kay, L. E. (2006) Isotope labeling strategies for the study of high-molecular-weight proteins by solution NMR spectroscopy. *Nat. Protoc. 1*, 749–754.
56. Cobine, P. A., George, G. N., Winzor, D. J., Harrison, M. D., Mogahaddas, S., and Dameron, C. T. (2000) Stoichiometry of complex formation between copper(I) and the N-terminal domain of the Menkes protein. *Biochemistry 39*, 6857–6863.
57. Ralle, M., Lutsenko, S., and Blackburn, N. J. (2004) Copper transfer to the N-terminal domain of the Wilson disease protein (ATP7B): X-ray absorption spectroscopy of reconstituted and chaperone-loaded metal binding domains and their interaction with exogenous ligands. *J. Inorg. Biochem. 98*, 765–774.
58. Rodriguez-Granillo, A., Crespo, A., and Wittung-Stafshede, P. (2010) Interdomain interactions modulate collective dynamics of the metal-binding domains in the Wilson disease protein. *J.Phys. Chem. B 114*, 1836–1848.
59. O'Halloran, T. V. (1993) Transition metals in control of gene expression. *Science 261*, 715–725.
60. Mittag, T., Kay, L. E., and Forman-Kay, J. D. (2010) Protein dynamics and conformational disorder in molecular recognition. *J. Mol. Recognit. 23*, 105–116.
61. Forman-Kay, J. D. (1999) The "dynamics" in the thermodynamics of binding. *Nat. Struct. Biol. 6*, 1086–1087.